

Geodesic bound of the minimum energy expense to achieve membrane separation within finite time

Jin-Fu Chen,^{1,2,3} Ruo-Xun Zhai,² C. P. Sun,^{1,2} and Hui Dong^{2,*}

¹Beijing Computational Science Research Center, Beijing 100193, China

²Graduate School of China Academy of Engineering Physics,

No. 10 Xibeiwang East Road, Haidian District, Beijing, 100193, China

³now at: School of Physics, Peking University, Beijing 100871, China

(Dated: September 16, 2022)

To accomplish a task within limited operation time typically requires an excess expense of energy, whose minimum is of practical importance for the optimal design in various applications, especially in the industrial separation of mixtures for purification of components. Technological progress has been made to achieve better purification with lower energy expense, yet little is known about the fundamental limit on the least excess energy expense in finite operation time. We derive such a limit and show its proportionality to the square of a geometric distance between the initial and final states and inverse proportionality to the operation time τ . Our result demonstrates that optimizing the separation protocol is equivalent to finding the geodesic curve in a geometric space. Interestingly, we show the optimal control with the minimum energy expense is achieved by a symmetry-breaking protocol, where the two membranes are moved toward each other with different speeds.

Separating components in a chemical mixture into their purer forms is critical in industrial applications [1], such as water purification [2–4], pharmaceutical and biological industry [5, 6], and the environmental science of CO₂ controls [7–10]. The membrane separation is one of the most promising technologies due to its low energy consumption and environmental-friendly operation [11–16]. Significant efforts have been made to improve the efficiency of the membranes from the perspective of material design [14, 16]. Nevertheless, the extent to which these properties benefit the energy expense in separation processes remains elusive. An important question arising naturally is whether there is a lower bound to the energy consumption posted by the basic laws of thermodynamics. If so, such a bound shall shed light on the material synthesis and the protocol design of separation processes.

We seek a fundamental bound of the least energy expense in finite operation time as a consequence of the basic law of thermodynamics, particularly the geometric structure of the thermal equilibrium configuration space [17–24]. For quasi-static processes with infinite operation time, the basic laws of thermodynamics have already provided a universal lower bound for the energy consumption: the performed work should exceed the free energy change of the separated final state and the mixed initial state $W \geq \Delta F$ [25, 26]. For a practical finite-time separation process, an excess work beyond the quasi-static separation is typically required [15, 26, 27] and should be optimized to reach the fundamental limit [27–30]. We convert such a task of finding the minimum energy expense into finding the shortest path in a configuration space, demonstrating the first application of geometric optimization in the membrane separation process.

Modeling the membrane separation. Consider a binary mixture of molecules in a chamber with volume V_t , as illustrated in Fig. 1(a). The system is immersed

in a thermal bath with temperature T_0 . Two species of the molecules are shown as red balls (type- α) and blue triangular pyramids (type- β) with the numbers of the molecules N_α and N_β . The separation process is performed by mechanically moving two semipermeable membranes A and B from the two ends towards each other. The membrane A (B) is designed with the properties allowing only type- α (type- β) molecules to penetrate. The chamber is divided into three compartments with the two membranes: the left one with volume V_L for the purified type- α molecules, the middle one with volume V_M for the molecular mixture, and the right one with volume V_R for the purified type- β molecules. The three volumes satisfy the condition $V_L + V_M + V_R = V_t$. At the end of the separation, the two membranes A and B contact each other, i.e. $V_M = 0$, and the two gases are purified in the left and the right compartments.

We denote the number of type- σ ($\sigma = \alpha, \beta$) molecules in the compartment k ($k = L, M, R$) as $N_{\sigma k}$. The impermeability of membrane A (B) to type- α (type- β) molecules results in $N_{\beta L} = N_{\alpha R} = 0$. For the gaseous molecules, the relaxation time is far shorter than the operation time, typically referenced as the endo-reversible region [31, 32], where the status of the gas can be described by macroscopic parameters, i.e., the pressure and the temperature. We assume the heat exchange inside the system is fast enough to ensure a global temperature T for the molecules in the whole chamber. It is worth noting that the temperature T typically differs from the bath temperature T_0 due to the finite-time operation. The equation of state for the gases in each compartment is

$$p_{\sigma k} V_k = N_{\sigma k} k_B T, \quad (1)$$

where k_B is the Boltzmann constant, and $p_{\sigma k}$ is the corresponding partial pressure.

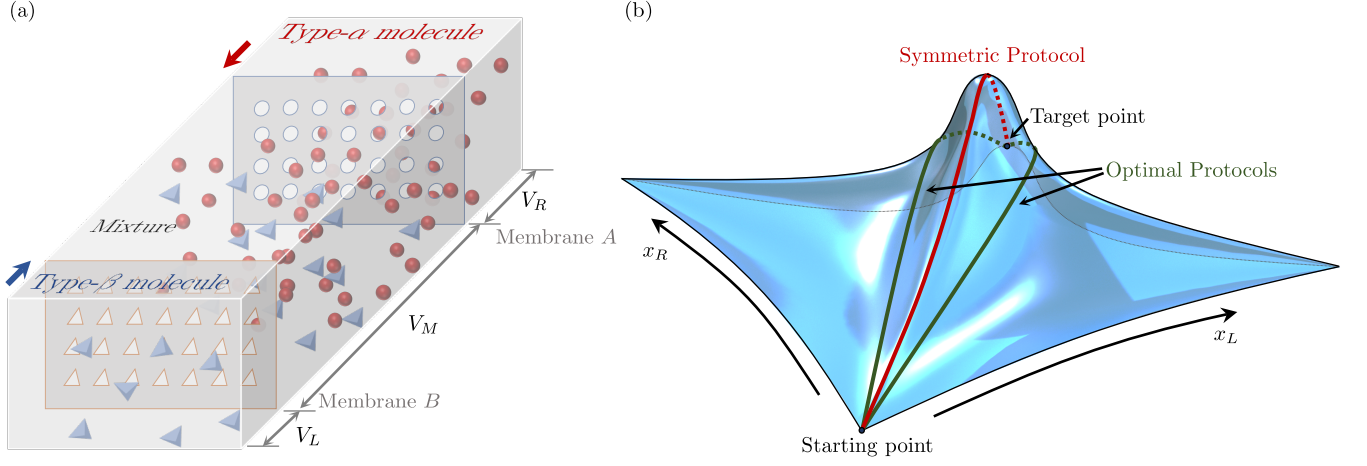


Figure 1. Separation of binary mixed gases. (a) The schematic of the separation process. The mixture consists of two types of molecules, type- α (red balls) and type- β (blue triangular pyramids). The semipermeable membrane A (B) is designed for only type- α (β) to pass through. The chamber is divided into three compartments, the left one (with volume V_L) for the purified type- α molecules, the middle one (with volume V_M) for the molecular mixture, and the right one (with volume V_R) for the purified type- β molecules. The two membranes are pushed towards each other during the separation process. (b) Sketch of the landscape of the configuration space spanned by $x_k = V_k/V_t$ ($k = L, R$) for the separation process. The metric is reflected by the surface in the three-dimensional space with an example of the equally mixed gases with symmetric diffusion coefficient. The excess work is reflected by the length of the path between the start point $(0, 0)$ and the target point $(0.5, 0.5)$.

Two types of relaxations exist in the separation process, the particle transport across the membranes and the heat conduction through the wall of the chamber. According to Fick's law [33], the particle transport flux \mathcal{J}_α (\mathcal{J}_β) of type- α (type- β) molecules across the membrane A (B) is proportional to the particle-density difference $\Delta c_\alpha = N_{\alpha M}/V_M - N_{\alpha L}/V_L$ ($\Delta c_\beta = N_{\beta M}/V_M - N_{\beta R}/V_R$) across the membrane A (B), namely, $\mathcal{J}_\alpha = \mu_\alpha \Delta c_\alpha$ and $\mathcal{J}_\beta = \mu_\beta \Delta c_\beta$, where μ_α (μ_β) is the diffusion coefficient of the type- α (type- β) molecules penetrating membrane A (B). The change rates of the molecular numbers are described by $\dot{N}_{\alpha L} = \mathcal{J}_\alpha \mathcal{A}$ and $\dot{N}_{\beta R} = \mathcal{J}_\beta \mathcal{A}$, and are explicitly

$$\begin{aligned} \dot{N}_{\alpha L} &= \mu_\alpha \mathcal{A} \left(\frac{N_{\alpha M}}{V_M} - \frac{N_{\alpha L}}{V_L} \right), \\ \dot{N}_{\beta R} &= \mu_\beta \mathcal{A} \left(\frac{N_{\beta M}}{V_M} - \frac{N_{\beta R}}{V_R} \right), \end{aligned} \quad (2)$$

where \mathcal{A} is the area of membranes, assumed the same for both membranes A and B. We adopt Newton's law of cooling to describe the heat conduction between the system and the thermal bath, i.e. $\dot{Q} = -C_V \gamma (T - T_0)$. Here C_V is the heat capacity of the system at constant volume, e.g. $C_V = 3/2 N_t k_B$ for the ideal single-atom gas. $N_t = N_\alpha + N_\beta$ is the total number of the two types of molecules. γ is the cooling rate of the system. With the first law of thermodynamics, the evolution of the gas temperature T is described as

$$C_V \dot{T} = -C_V \gamma (T - T_0) + \dot{W}, \quad (3)$$

where \dot{W} is the mechanical work rate performed on the gas while moving the membranes.

Excess energy expense. To accomplish the separation, the mechanical work performed by moving the membranes is

$$W = - \int_0^\tau \sum_{\sigma=\alpha,\beta} \sum_{k=L,M,R} p_{\sigma k} \dot{V}_k dt, \quad (4)$$

where τ is the operation time of the separation process and $\dot{V}_k = dV_k/dt$ is the volume change rate of the compartment k . For convenience, we define two dimensionless parameters determining the configuration of the system, $x_L \equiv V_L/V_t$ and $x_R \equiv V_R/V_t$. The two species of molecules are completely mixed initially with $x_L(0) = x_R(0) = 0$. They are separated finally with $x_L(\tau)$ and $x_R(\tau)$ satisfying $x_L(\tau) + x_R(\tau) = 1$. During the separation, there is a constraint condition $0 \leq x_L(t) + x_R(t) \leq 1$.

For the quasi-static separation with infinite time τ , the minimum work is reached as $W_{\min}^{(0)} = -N_t k_B T_0 (\epsilon_\alpha \ln \epsilon_\alpha + \epsilon_\beta \ln \epsilon_\beta)$ by choosing the final volume proportional to the ratio $\epsilon_\sigma \equiv N_\sigma/N_t$ of the two gases, namely, $x_L(\tau) = \epsilon_\alpha$ and $x_R(\tau) = \epsilon_\beta$. See Supplementary Material for detailed discussion. For slow processes with long operation time τ , the leading term of the excess work rate is a quadratic form

$$\begin{aligned} \dot{W}_{\text{ex}} = & \frac{2N_t k_B T_0}{3\gamma} \left[\frac{\epsilon_\alpha \dot{x}_R}{1-x_R} + \frac{\epsilon_\beta \dot{x}_L}{1-x_L} \right]^2 \\ & + \frac{N_t k_B T_0 V_t}{\mathcal{A}} \left\{ \frac{\epsilon_\alpha (1-x_R)}{\mu_\alpha} \left[\frac{d}{dt} \left(\frac{x_L}{1-x_R} \right) \right]^2 \right. \\ & \left. + \frac{\epsilon_\beta (1-x_L)}{\mu_\beta} \left[\frac{d}{dt} \left(\frac{x_R}{1-x_L} \right) \right]^2 \right\}. \end{aligned} \quad (5)$$

The first term shows the contribution due to the temperature difference between the system and the bath during the finite-time separation process. The second term shows the contribution due to the particle-density difference across the membranes A and B.

Riemann geometry of the configuration space. The quadratic form of excess work \dot{W}_{ex} in Eq. (5) allows the definition of a geometric length in the configuration space spanned by (x_L, x_R) . We introduce the timescale of heat transfer $\tau_h \equiv 1/\gamma$ and that of particle transport of type- σ molecules $\tau_\sigma \equiv V_t/(\mu_\sigma \mathcal{A})$, and rewrite Eq. (5) into a compact form

$$\dot{W}_{\text{ex}} = (\dot{x}_L \ \dot{x}_R) G \begin{pmatrix} \dot{x}_L \\ \dot{x}_R \end{pmatrix}, \quad (6)$$

where G is the metric of the current Riemann manifold

$$G = \begin{pmatrix} g_{LL} & g_{LR} \\ g_{RL} & g_{RR} \end{pmatrix}, \quad (7)$$

with the components $g_{LL} = N_t k_B T_0 [\epsilon_\beta \tau_\beta x_R^2 / (1-x_L)^3 + \epsilon_\alpha \tau_\alpha / (1-x_R) + 2/3 \cdot \epsilon_\beta^2 \tau_h / (1-x_L)^2]$, $g_{LR} = g_{RL} = N_t k_B T_0 [\epsilon_\alpha \tau_\alpha x_L / (1-x_R)^2 + \epsilon_\beta \tau_\beta x_R / (1-x_L)^2 + 2/3 \cdot \epsilon_\alpha \epsilon_\beta \tau_h / (1-x_L)(1-x_R)]$, $g_{RR} = N_t k_B T_0 [\epsilon_\alpha \tau_\alpha x_L^2 / (1-x_R)^3 + \epsilon_\beta \tau_\beta / (1-x_L) + 2/3 \cdot \epsilon_\alpha^2 \tau_h / (1-x_R)^2]$.

The protocol of the separation process is given by $\tilde{x}_L(s) = x_L(t)$ and $\tilde{x}_R(s) = x_R(t)$ with the rescaled time $s \equiv t/\tau$, $0 \leq s \leq 1$. The protocol $\tilde{x}_L(s)$ and $\tilde{x}_R(s)$ can be designed to minimize the excess work with fixed operation time τ along a given path $\mathcal{P}(x_L, x_R) = 0$ in the configuration space. With the Cauchy-Schwarz inequality

According to Eq. (9), the thermodynamic length of the symmetric path as a function of the endpoint coordinate $x(\tau)$ is obtained as

$$\begin{aligned} \mathcal{L}_s(x(\tau)) = & \int_0^{x(\tau)} \sqrt{g_{LL}(x, x) dx^2 + g_{LR}(x, x) dx^2 + g_{RL}(x, x) dx^2 + g_{RR}(x, x) dx^2} \\ = & 2\sqrt{N_t k_B T_0} \left(\sqrt{\frac{\tau_p}{1-x} + \frac{2}{3}\tau_h} - \sqrt{\frac{2\tau_h}{3}} \sinh^{-1} \sqrt{\frac{2(1-x)\tau_h}{3\tau_p}} \right) \Big|_{x=0}^{x(\tau)} \end{aligned} \quad (11)$$

By setting $x(\tau) = 0.5$, we obtain the length of the whole path $\mathcal{L}_{\text{sym}} = \mathcal{L}_s(0.5)$.

The lower bound of excess work for symmetric proto-

$\int_0^\tau \dot{W}_{\text{ex}} dt \int_0^\tau dt \geq (\int_0^\tau \sqrt{\dot{W}_{\text{ex}}} dt)^2 \equiv \mathcal{L}^2$, the excess work of the given path with different protocols is bounded by

$$W_{\text{ex}} \geq \frac{\mathcal{L}^2}{\tau}, \quad (8)$$

where the thermodynamic length $\mathcal{L} = \int_0^\tau \sqrt{\dot{W}_{\text{ex}}} dt$ is only determined by the path \mathcal{P} in the configuration space [19, 21]

$$\mathcal{L} = \int_{\mathcal{P}} \sqrt{(dx_L \ dx_R) G \begin{pmatrix} dx_L \\ dx_R \end{pmatrix}}. \quad (9)$$

The equality is reached for the protocol with a constant work rate $\dot{W}_{\text{ex}} = \text{const}$ or a constant velocity of the thermodynamic length $d\mathcal{L}/ds = \text{const}$. The task to seek the minimum energy consumption in finite time is converted into searching geodesic paths connecting the start point $(0, 0)$ and the target point $(\epsilon_\alpha, \epsilon_\beta)$ in the configuration space.

Geodesic paths in the current Riemann manifold are described by the geodesic equations,

$$\frac{d^2 x^k}{dr^2} + \Gamma^k_{ij} \frac{dx^i}{dr} \frac{dx^j}{dr} = 0, \quad i = 1, 2, \quad (10)$$

where the Einstein notation is employed, and $x^1 \equiv x_L$, $x^2 \equiv x_R$. We parameterize the geodesic paths with the arc length r by setting the initial condition $g_{ij} \frac{dx^i}{dr} \frac{dx^j}{dr} = 1$. The Christoffel symbols Γ^k_{ij} are obtained as $\Gamma^k_{ij} = \frac{1}{2} g^{kl} (\partial g_{li} / \partial x^j + \partial g_{lj} / \partial x^i - \partial g_{ij} / \partial x^l)$, where g^{kl} are the elements of the inverse metric G^{-1} . The explicit form of Γ^k_{ij} is shown in Supplementary Material.

Symmetric control path. For symmetric parameters $\tau_\alpha = \tau_\beta = \tau_p$, $\epsilon_\alpha = \epsilon_\beta = 0.5$, the symmetric path $x_L(t) = x_R(t) \equiv x(t) = \tilde{x}(t/\tau)$ is a geodesic path.

cols is $\mathcal{L}_{\text{sym}}^2/\tau$. To reach such bound, we obtain a protocol

$\tilde{x}(s)$ in an implicitly form as

$$\mathcal{L}_s(\tilde{x}(s)) = s\mathcal{L}_{\text{sym}}. \quad (12)$$

It can be verified that $x^1(r) = x^2(r) = \tilde{x}(r/\mathcal{L}_{\text{sym}})$ is a solution to the geodesic equations. We explicitly show two situations where relaxation of the particle transport or that of heat exchange dominates during the separation process.

(1) Particle transport dominated process ($\tau_h \ll \tau_p$). The temperature of the system is identical to that of the bath, $T = T_0$. The excess work rate is simplified as $\dot{W}_{\text{ex}} = N_t k_B T_0 \tau_p (1-x) \{d/dt[x/(1-x)]\}^2$. The thermodynamic length follows as $\mathcal{L} = (2\sqrt{2}-2)\sqrt{N_t k_B T_0 \tau_p}$. According to Eq. (8), the minimum excess work is

$$W_{\text{ex}}^{(\text{min})} = (12 - 8\sqrt{2})N_t k_B T_0 \frac{\tau_p}{\tau}.$$

The optimal protocol is designed as $\tilde{x}_L(s) = \tilde{x}_R(s) = 1 - [(\sqrt{2}-1)s+1]^{-2}$ to achieve the above minimum excess work.

(2) Heat exchange dominated process ($\tau_h \gg \tau_p$). The excess work rate is simplified into $\dot{W}_{\text{ex}} = 2/3 \cdot N_t k_B T_0 \tau_h [\dot{x}/(1-x)]^2$. The minimum excess work is

$$W_{\text{ex}}^{(\text{min})} = \frac{2(\ln 2)^2}{3} N_t k_B T_0 \frac{\tau_h}{\tau}. \quad (13)$$

The designed protocol is obtained as $\tilde{x}_L(s) = \tilde{x}_R(s) = 1 - 2^{-s}$. We summarize the two situations in Table I.

Symmetry breaking in the optimal separation protocol. The question arises that whether the straightforward symmetric protocol above is the optimal one with the minimum energy expense. Our answer is no. We find a symmetry-breaking protocol for the perfect symmetric setup to reach the minimum energy expense.

For given parameters, we use the shooting method [34] to numerically solve the geodesic path connecting the initial position (0,0) and the final position (0.5,0.5) in the configuration space. For room temperature $T_0 = 298.15\text{K}$, we consider the symmetric situation of two moles equally mixed gases with $N_t = 2N_A$, where N_A is the Avogadro constant. The particle transport relaxation timescales are the same $\tau_\alpha = \tau_\beta = 1\text{s}$, and the heat conduction relaxation timescale is $\tau_h = 0.1\text{s}$. We find three geodesic paths connecting the start point (0,0) and the target point (0.5,0.5), shown in Fig 2(a) as the symmetric red dashed line and the two green lines. To visualize the symmetry breaking of the control scheme in the optimal separation protocol, we sketch the three-dimensional embedding of the current two-dimensional Riemann manifold in Fig. 1(b), where the thermodynamic length is reflected by the length of the path. The symmetric and the symmetry-breaking geodesic paths are shown in red and green lines. The green lines are shorter than the red one, representing smaller excess work.

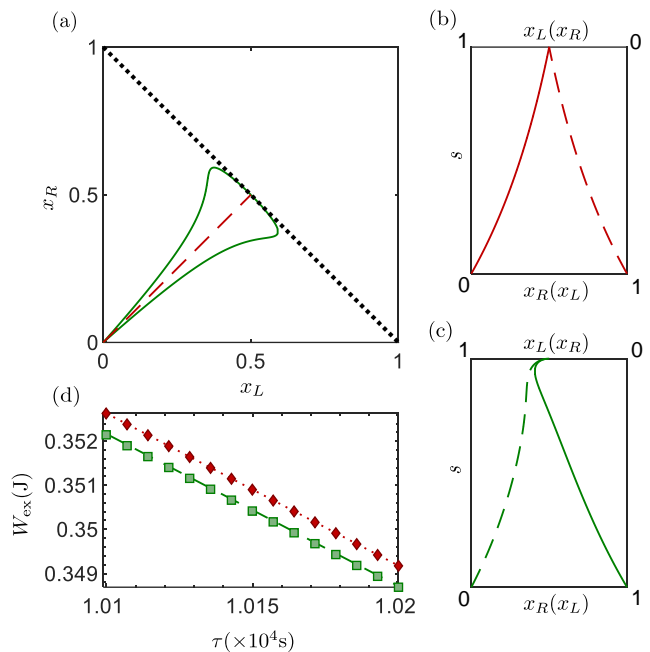


Figure 2. Symmetry-breaking protocol of the separation process with the minimum excess work. The permeable properties of membranes A and B to the corresponding type of molecules are the same, and the numbers of type- α and type- β molecules are equal. Namely, all the parameters of this system are symmetric ($\tau_\alpha = \tau_\beta = 1\text{s}$, $\tau_h = 0.1\text{s}$, $\epsilon_\alpha = \epsilon_\beta = 0.5$, $N_t = 2N_A$, $T_0 = 298.15\text{K}$, where N_A is the Avogadro constant). (a) Three geodesic paths connecting (0,0) and (0.5,0.5). The thermodynamic length of the two symmetry-breaking geodesic paths (green solid line) is $\mathcal{L}_{\text{geo}} = 59.64(\text{J} \cdot \text{s})^{1/2}$, which is shorter than that of the symmetric one (red dashed line) $\mathcal{L}_{\text{sym}} = 59.68(\text{J} \cdot \text{s})^{1/2}$. (b) and (c) Control schemes of the protocols of the symmetry-breaking and the symmetric paths. In the symmetry-breaking protocol, the two membranes approach each other at a position slightly different from the equilibrium position, and are moved together to the equilibrium position. (d) Excess work W_{ex} versus operation time τ . The red diamonds (green squares) represent the irreversible work obtained by solving the evolution equation of the system along the symmetric (symmetry-breaking) path. While the red dashed line (green solid line) represents the excess work predicted by the thermodynamic length $W_{\text{ex}} = \mathcal{L}^2/\tau$.

The red dashed line of symmetric protocol shown in Fig 2(a) has a thermodynamic length of $\mathcal{L}_{\text{sym}} = 59.68(\text{J} \cdot \text{s})^{1/2}$. The lengths of the symmetry-breaking green geodesic paths are $\mathcal{L}_{\text{geo}} = 59.64(\text{J} \cdot \text{s})^{1/2}$, shorter than the symmetric one. The control schemes $\tilde{x}_{L,R}(s)$ for the symmetric and symmetry-breaking protocol are shown in Fig. 2(b) and Fig. 2(c). In the symmetry-breaking protocol shown in Fig. 2(c), the two membranes approach each other at a position different from the equilibrium position, and then are moved together to the equilibrium position. In Fig. 2(d), we compares the results obtained with the quadratic form in Eq. (5)

Table I. Optimal separation protocol of equally mixed gases under the symmetric path to move two membranes. Two regions of the relaxation timescales are considered, (1) particle transport dominated process ($\tau_h \ll \tau_p$) and (2) heat exchange dominated process ($\tau_h \gg \tau_p$).

	$\tau_h \ll \tau_p$	$\tau_h \gg \tau_p$
$W_{\text{ex}}^{(\text{min})}$	$(12 - 8\sqrt{2})N_t k_B T_0 \frac{\tau_p}{\tau}$	$\frac{2(\ln 2)^2}{3} N_t k_B T_0 \frac{\tau_h}{\tau}$
Protocol	$\tilde{x}_L(s) = \tilde{x}_R(s) = 1 - [(\sqrt{2} - 1)s + 1]^{-2}$	$\tilde{x}_L(s) = \tilde{x}_R(s) = 1 - 2^{-s}$

and the numerical solution of the evolution equations (2) and (3). The red dotted line and the green dashed line show the approximate excess work predicted by thermodynamic length $W_{\text{ex}} = \mathcal{L}^2/\tau$. And the red diamonds and the green squares present the excess work calculated with Eq. (4) by solving the evolution Eqs. (2) and (3) for the corresponding protocols $V_{L,R}(t)$ obtained from the geodesic equations.

Conclusion. We prove the equivalence between designing optimum control to achieve the minimum energy expense and finding the geodesic path in a geometric space. Such an equivalence has also been exploited in the optimization of control protocols in stochastic and quantum thermodynamics [21–24]. With this equivalence, we show the minimum excess energy expense is proportional to the square of the length of that geodesic path and inversely proportional to the operation time τ . In a separation process where all the parameters are symmetric $\tau_\alpha = \tau_\beta = \tau_p$, $\epsilon_\alpha = \epsilon_\beta = 0.5$, we found three geodesic paths, among them a simple and straightforward path is symmetric in the configuration space (x_L, x_R) . The corresponding protocol is to move the two membranes with the same speed. In this situation, we predict that the complete separation of equally mixed single-atom gases requires excess work at least $(12 - 8\sqrt{2})N_t k_B T_0 \tau_p/\tau$ for the particle transport dominated process and $2(\ln 2)^2 N_t k_B T_0 \tau_h/(3\tau)$ for the heat exchange dominated process, where τ_p and τ_h are the relaxation time for the particle transport and the heat exchange.

Importantly, the current work shows that such symmetric protocol is not the best one to achieve the minimal energy expense. A symmetry-breaking protocol is the optimal protocol that achieves the lowest energy expense for given operation time τ . In the optimal protocol, one membrane is moved faster than the other, the membranes approach each other at a position slightly deviated from the equilibrium position. Then they are moved together to the equilibrium position.

Acknowledgments. This work is supported by the National Natural Science Foundation of China (NSFC) (Grants No. 12088101, No. 11534002, No. 11875049, No. U1930402, No. U1930403 and No. 12047549) and the National Basic Research Program of China (Grant No. 2016YFA0301201).

Jin-Fu Chen and Ruo-Xun Zhai contributed equally to this work.

* hdong@g scaep.ac.cn

- [1] David S. Sholl and Ryan P. Lively, “Seven chemical separations to change the world,” *Nature* **532**, 435–437 (2016).
- [2] William J. Koros and Ryan P. Lively, “Water and beyond: Expanding the spectrum of large-scale energy efficient separation processes,” *AIChE Journal* **58**, 2624–2633 (2012).
- [3] Pedro J. J. Alvarez, Candace K. Chan, Menachem Elimelech, Naomi J. Halas, and Dino Villagrán, “Emerging opportunities for nanotechnology to enhance water security,” *Nat. Nanotechnol.* **13**, 634–641 (2018).
- [4] Sadaf Noamani, Shirin Niroomand, Masoud Rastgar, and Mohtada Sadrzadeh, “Carbon-based polymer nanocomposite membranes for oily wastewater treatment,” *npj Clean Water* **2**, 20 (2019).
- [5] Robert van Reis and Andrew Zydney, “Bioprocess membrane technology,” *J. Membr. Sci.* **297**, 16–50 (2007).
- [6] Rui Xie, Liang-Yin Chu, and Jin-Gen Deng, “Membranes and membrane processes for chiral resolution,” *Chem. Soc. Rev.* **37**, 1243 (2008).
- [7] H. Dannström O. Falk-Pedersen, “Separation of carbon dioxide from offshore gas turbine exhaust,” *Energy Conversion and Management* **38**, S81–S86 (1997).
- [8] Eric Favre, “Carbon dioxide recovery from post-combustion processes: Can gas permeation membranes compete with absorption?” *Journal of Membrane Science* **294**, 50–59 (2007).
- [9] Tim C. Merkel, Haiqing Lin, Xiaotong Wei, and Richard Baker, “Power plant post-combustion carbon dioxide capture: An opportunity for membranes,” *Journal of Membrane Science* **359**, 126–139 (2010).
- [10] J.K. Adewole, A.L. Ahmad, S. Ismail, and C.P. Leo, “Current challenges in membrane separation of CO2 from natural gas: A review,” *International Journal of Greenhouse Gas Control* **17**, 46–65 (2013).
- [11] I.M. Britan, I.L. Leites, and T.N. Vasilkovskaya, “Membrane technology of mixed-gas separation: thermodynamic analysis for feasibility study,” *J. Membr. Sci.* **55**, 349–352 (1991).
- [12] W.J. Koros and G.K. Fleming, “Membrane-based gas separation,” *J. Membr. Sci.* **83**, 1–80 (1993).
- [13] Robert Spillman, “Chapter 13 economics of gas separation membrane processes,” in *Membrane Science and Technology* (Elsevier, 1995) pp. 589–667.
- [14] Anil Kumar Pabby, Syed S. H. Rizvi, and Ana Maria Sastre Requena, *Handbook of Membrane Separations Chemical, Pharmaceutical, Food, and Biotechnological Applications, Second Edition* (Taylor and Francis Group, 2015) p. 878.

- [15] Christophe Castel and Eric Favre, “Membrane separations and energy efficiency,” *J. Membr. Sci.* **548**, 345–357 (2018).
- [16] Mihir K. Purkait and Randeep Singh, *Membrane Technology in Separation Science* (Taylor and Francis Group, 2018) p. 242.
- [17] F. Weinhold, “Metric geometry of equilibrium thermodynamics,” *J. Chem. Phys.* **63**, 2479–2483 (1975).
- [18] George Ruppeiner, “Thermodynamics: A riemannian geometric model,” *Phys. Rev. A* **20**, 1608–1613 (1979).
- [19] Peter Salamon and R. Stephen Berry, “Thermodynamic length and dissipated availability,” *Phys. Rev. Lett.* **51**, 1127–1130 (1983).
- [20] Gavin E. Crooks, “Measuring thermodynamic length,” *Phys. Rev. Lett.* **99**, 100602 (2007).
- [21] David A. Sivak and Gavin E. Crooks, “Thermodynamic metrics and optimal paths,” *Phys. Rev. Lett.* **108**, 190602 (2012).
- [22] Matteo Scandi and Martí Perarnau-Llobet, “Thermodynamic length in open quantum systems,” *Quantum* **3**, 197 (2019).
- [23] Jin-Fu Chen, C. P. Sun, and Hui Dong, “Extrapolating the thermodynamic length with finite-time measurements,” *Phys. Rev. E* **104**, 034117 (2021).
- [24] Geng Li, Jin-Fu Chen, C.P. Sun, and Hui Dong, “Geodesic path for the minimal energy cost in shortcuts to isothermality,” *Phys. Rev. Lett.* **128**, 230603 (2022).
- [25] Herbert B. Callen, *Thermodynamics and an Introduction to Thermostatistics*, 2nd ed. (Wiley, 1985).
- [26] Kerson Huang, *Statistical mechanics*, 2nd ed. (Wiley, 1987).
- [27] Anatoliy M. Tsirlin, Vladimir Kazakov, and Dmitrii V. Zubov, “Finite-time thermodynamics: limiting possibilities of irreversible separation processes†,” *J. Phys. Chem. A* **106**, 10926–10936 (2002).
- [28] Jianguo Xu and Rakesh Agrawal, “Membrane separation process analysis and design strategies based on thermodynamic efficiency of permeation,” *Chem. Eng. Sci.* **51**, 365–385 (1996).
- [29] Stanislaw Sieniutycz and Anatoly Tsirlin, “Finding limiting possibilities of thermodynamic systems by optimization,” *Phil. trans. R. Soc. A* **375**, 20160219 (2017).
- [30] Stanislaw Sieniutycz and Jacek Jeżowski, “Optimization and qualitative aspects of separation systems,” in *Energy Optimization in Process Systems and Fuel Cells* (Elsevier, 2018) pp. 273–333.
- [31] F. L. Curzon and B. Ahlborn, “Efficiency of a carnot engine at maximum power output,” *Am. J. Phys* **43**, 22–24 (1975).
- [32] Peter Salamon and Abraham Nitzan, “Finite time optimizations of a newton’s law carnot cycle,” *J. Chem. Phys.* **74**, 3546–3560 (1981).
- [33] Bertil Hille, *Ion Channels of Excitable Membranes* (Sinauer Associates is an imprint of Oxford University Press, 2001).
- [34] Marcel Berger, *A Panoramic View of Riemannian Geometry* (Springer Berlin Heidelberg, 2007).

Supplementary Material: Geodesic bound of the minimum energy expense to achieve membrane separation within finite time

Jin-Fu Chen,^{1,2,3} Ruo-Xun Zhai,² Chang-Pu Sun,^{1,2} and Hui Dong^{2,*}

¹Beijing Computational Science Research Center, Beijing 100193, China

²Graduate School of China Academy of Engineering Physics,

No. 10 Xibeiwang East Road, Haidian District, Beijing, 100193, China

³now at: School of Physics, Peking University, Beijing 100871, China

(Dated: September 16, 2022)

The document is devoted to providing the detailed derivation and the discussions to the main text.

I. FIRST-ORDER APPROXIMATION FOR EVOLUTION EQUATION

The quadratic form of \dot{W}_{ex} is obtained by keeping the series solutions of evolution equations to the first-order term of $1/\tau$. The approximation is validated when the time of process τ is much larger than the relaxation time of the system $\tau_{\alpha,\beta}$ and τ_h , or in the endo-reversible region. For a given protocol $\tilde{x}_k(s)$, $V_k(t)$ is obtained by $V_k(t) = V_t \tilde{x}_k(t/\tau)$, ($k = L, R$). The time evolution of the system are described by Eqs. (1) - (3). We define the variation of $N_{\sigma k}$ and T from the corresponding equilibrium states as

$$\Delta N_{\alpha L} \equiv N_{\alpha L} - \frac{V_L}{V_M + V_L} N_{\alpha}, \quad \Delta N_{\beta R} \equiv N_{\beta R} - \frac{V_R}{V_M + V_R} N_{\beta}, \quad \Delta T \equiv T - T_0. \quad (\text{S1})$$

The evolution equations of the variations are

$$\frac{d}{dt}(\Delta N_{\alpha L}) = -N_{\alpha} \frac{d}{dt} \left(\frac{V_L}{V_M + V_L} \right) - \mu_{\alpha A} \mathcal{A} \left(\frac{1}{V_M} + \frac{1}{V_L} \right) \Delta N_{\alpha L}, \quad (\text{S2})$$

$$\frac{d}{dt}(\Delta N_{\beta R}) = -N_{\beta} \frac{d}{dt} \left(\frac{V_R}{V_M + V_R} \right) - \mu_{\beta B} \mathcal{A} \left(\frac{1}{V_M} + \frac{1}{V_R} \right) \Delta N_{\beta R}, \quad (\text{S3})$$

$$\frac{d}{dt}(\Delta T) = -\gamma \Delta T + \frac{k_B(T_0 + \Delta T)}{C_V} f(t), \quad (\text{S4})$$

where $f(t) \equiv \dot{V}_L \left[N_{\beta} / (V_M + V_R) - (1/V_M + 1/V_L) \Delta N_{\alpha L} - \Delta N_{\beta R} / V_M \right] + \dot{V}_R \left[N_{\alpha} / (V_M + V_L) - (1/V_M + 1/V_R) \Delta N_{\beta R} - \Delta N_{\alpha L} / V_M \right]$. To the first-order term of $1/\tau$, Eqs. (S2)-(S4) are solved by self-iteration method,

$$\begin{aligned} \Delta N_{\alpha L}(t) &\approx - \frac{N_{\alpha}}{\mu_{\alpha A} \mathcal{A} \left(\frac{1}{V_M} + \frac{1}{V_L} \right)} \frac{d}{dt} \left(\frac{V_L}{V_t - V_R} \right), \\ \Delta N_{\beta R}(t) &\approx - \frac{N_{\beta}}{\mu_{\beta B} \mathcal{A} \left(\frac{1}{V_M} + \frac{1}{V_R} \right)} \frac{d}{dt} \left(\frac{V_R}{V_t - V_L} \right), \\ \Delta T(t) &\approx \frac{k_B T_0}{\gamma C_V} \left(\frac{\dot{V}_L}{V_t - V_L} N_{\beta} + \frac{\dot{V}_R}{V_t - V_R} N_{\alpha} \right). \end{aligned} \quad (\text{S5})$$

The details of iteration method are presented in the Supplementary Information.

II. EXCESS WORK RATE

The work rate of the system is $\dot{W} = \sum_{\sigma=\alpha,\beta} \sum_{k=L,M,R} p_{\sigma k} \dot{V}_k = -p_{\alpha L} \dot{V}_L - p_{\beta R} \dot{V}_R - (p_{\alpha M} + p_{\beta M})(-\dot{V}_L - \dot{V}_R)$. Together with Eq. (1), the work rate is expressed as

$$\dot{W} = k_B T \dot{V}_L \left(\frac{N_{\alpha M}}{V_M} + \frac{N_{\beta M}}{V_M} - \frac{N_{\alpha L}}{V_L} \right) + k_B T \dot{V}_R \left(\frac{N_{\alpha M}}{V_M} + \frac{N_{\beta M}}{V_M} - \frac{N_{\beta R}}{V_R} \right). \quad (\text{S6})$$

Substituting Eq. (S5) into Eq. (S6) and keeping to quadratic term of $1/\tau$, we obtain the leading term of the total work rate, which is divided into the reversible part and excess part, i.e., $\dot{W} = \dot{W}^{(0)} + \dot{W}_{\text{ex}}$. In reversible separation processes, the system stays at a transient equilibrium state at every moment, the partial pressures of type- α (type- β) molecules over the A (B) membrane are equal $p_{\alpha L} = p_{\alpha M}, p_{\beta R} = p_{\beta M}$, then all the work done during this process is reversible, and the work rate is

$$\dot{W}^{(0)} = k_B T_0 \left(\dot{V}_L \cdot \frac{N_\beta}{V_t - V_L} + \dot{V}_R \cdot \frac{N_\alpha}{V_t - V_R} \right).$$

The excess work rate is obtained by subtracting the reversible one $\dot{W}^{(0)}$ from \dot{W} , i.e., $\dot{W}_{\text{ex}} = \dot{W} - \dot{W}^{(0)}$, and the result is given by Eq. (5).

III. MINIMAL REVERSIBLE WORK

For the quasi-static isothermal separation with infinite operation time, the partial pressure of molecules in each compartment satisfies $p_{\alpha M} = p_{\alpha L}$ and $p_{\beta M} = p_{\beta R}$. The molecular number of the gas in each compartment is

$$N_{\alpha L} = N_\alpha \frac{V_L}{V_L + V_M}, \quad (\text{S7})$$

$$N_{\beta R} = N_\beta \frac{V_R}{V_R + V_M}, \quad (\text{S8})$$

with $N_{\alpha M} = N_\alpha - N_{\alpha L}$ and $N_{\beta M} = N_\beta - N_{\beta R}$. The temperature of the system remains the same as that of the bath $T = T_0$. The partial pressure $p_{\alpha M} = N_{\alpha M} k_B T_0 / (V_M + V_L)$ and $p_{\beta M} = N_{\beta M} k_B T_0 / (V_M + V_R)$ in the quasi-static process only depends on the volumes V_k ($k = L, M, R$) of the compartments. We set the final volumes of the left and the right compartments to be $V_L(\tau)$ and $V_R(\tau)$ with $V_L(\tau) + V_R(\tau) = V_t$. The performed work for the quasi-static process is

$$W^{(0)} = -k_B T_0 \left(N_\alpha \ln \frac{V_L(\tau)}{V_t} + N_\beta \ln \frac{V_R(\tau)}{V_t} \right). \quad (\text{S9})$$

The minimal quasi-static performed work is $W_{(0)}^{\text{min}} = -N_t k_B T_0 [\epsilon_\alpha \ln \epsilon_\alpha + \epsilon_\beta \ln \epsilon_\beta]$, which is reached by choosing $V_L(\tau)/V_t = \epsilon_\alpha \equiv N_\alpha/N$ and $V_R(\tau)/V_t = \epsilon_\beta \equiv N_\beta/N$. For the situation in the main text where $N_t = 2N_A, \epsilon_\alpha = \epsilon_\beta = 0.5, T_0 = 298.15\text{K}$, the minimal reversible work is $W^{(0)} = 3.44 \times 10^3 \text{J}$.

IV. SELF-ITERATION METHOD TO SOLVE DIFFERENTIAL EQUATIONS

We employ the self-iteration method to Eqs. (15)-(17) of the main text. We rewrite Eq. (15) into

$$\Delta N_{\alpha L} = - \frac{N_\alpha}{\mu_\alpha \mathcal{A} \left(\frac{1}{V_M} + \frac{1}{V_L} \right)} \frac{d}{dt} \left(\frac{V_L}{V_M + V_L} \right) - \frac{1}{\mu_\alpha \mathcal{A} \left(\frac{1}{V_M} + \frac{1}{V_L} \right)} \frac{d}{dt} (\Delta N_{\alpha L}).$$

The left hand side is the variable itself, while its time derivative is on the right hand side. By self-iterating the equation, we obtain a solution in the series form

$$\begin{aligned} \Delta N_{\alpha L} &= - \frac{N_\alpha}{\mu_\alpha \mathcal{A} \left(\frac{1}{V_M} + \frac{1}{V_L} \right)} \frac{d}{dt} \left(\frac{V_L}{V_M + V_L} \right) \\ &\quad - \frac{N_\alpha}{\mu_\alpha \mathcal{A} \left(\frac{1}{V_M} + \frac{1}{V_L} \right)} \frac{d}{dt} \left\{ - \frac{N_\alpha}{\mu_\alpha \mathcal{A} \left(\frac{1}{V_M} + \frac{1}{V_L} \right)} \frac{d}{dt} \left(\frac{V_L}{V_M + V_L} \right) - \frac{1}{\mu_\alpha \mathcal{A} \left(\frac{1}{V_M} + \frac{1}{V_L} \right)} \frac{d}{dt} (\Delta N_{\alpha L}) \right\} \\ &= N_\alpha \sum_{n=1}^{\infty} \left[- \frac{1}{\mu_\alpha \mathcal{A} \left(\frac{1}{V_M} + \frac{1}{V_L} \right)} \frac{d}{dt} \right]^n \left(\frac{V_L}{V_M + V_L} \right). \end{aligned}$$

We choose a given protocol to control the volume $V_k(t) = V_t \tilde{x}_k(t/\tau)$ with the operation time τ of the whole separation process. The time derivative is substituted into

$$\frac{d^n}{dt^n} x_k(t) = \frac{d^n}{dt^n} \tilde{x}_k(t/\tau) = \frac{1}{\tau^n} \frac{d^n}{ds^n} \tilde{x}_k(s), \quad (\text{S10})$$

with the rescaled time $s = t/\tau$. Therefore, each time derivative contributes a $1/\tau$ factor. For slow separation process, we keep to the lowest-order term of $1/\tau$, and obtain an approximate solution in Eq. (18) of the main text. The approximate solutions to $\Delta N_{\beta R}$ and ΔT can be obtained similarly.

V. SOLVING THE GEODESIC EQUATIONS

In this section, we show the method to numerically evaluate the geodesics paths connecting $(0, 0)$ and $(\epsilon_\alpha, \epsilon_\beta)$. We need to solve the geodesic equations

$$\frac{d^2 x^k}{dr^2} + \Gamma_{ij}^k \frac{dx^i}{dr} \frac{dx^j}{dr} = 0, \quad (\text{S11})$$

where (x^1, x^2) represents the coordinate (x_L, x_R) in the Riemann configuration space. The repeated indexes are summed. The expressions of elements of the metric are explicitly

$$\begin{aligned} g_{11} &= N_t k_B T_0 \left[\epsilon_\beta \tau_\beta (x^2)^2 / (1 - x_1)^3 + \epsilon_\alpha \tau_\alpha / (1 - x_2) + 2/3 \cdot \epsilon_\beta^2 \tau_h / (1 - x_1)^2 \right], \\ g_{12} = g_{21} &= N_t k_B T_0 \left[\epsilon_\alpha \tau_\alpha x^1 / (1 - x^2)^2 + \epsilon_\beta \tau_\beta x^2 / (1 - x^1)^2 + 2/3 \cdot \epsilon_\alpha \epsilon_\beta \tau_h / (1 - x^1)(1 - x^2) \right], \\ g_{22} &= N_t k_B T_0 \left[\epsilon_\alpha \tau_\alpha (x^1)^2 / (1 - x^2)^3 + \epsilon_\beta \tau_\beta / (1 - x^1) + 2/3 \cdot \epsilon_\alpha^2 \tau_h / (1 - x^2)^2 \right]. \end{aligned} \quad (\text{S12})$$

The Christoffel symbols are obtained as

$$\Gamma_{111} = \frac{N_t k_B T_0}{2} \left[\frac{4}{3} \cdot \frac{\epsilon_\beta^2 \tau_h}{(1 - x^1)^3} + \frac{3 \epsilon_\beta \tau_\beta (x^2)^2}{(1 - x^1)^4} \right], \quad (\text{S13})$$

$$\Gamma_{222} = \frac{N_t k_B T_0}{2} \left[\frac{4}{3} \cdot \frac{\epsilon_\alpha^2 \tau_h}{(1 - x^2)^3} + \frac{3 \epsilon_\alpha \tau_\alpha (x^1)^2}{(1 - x^2)^4} \right], \quad (\text{S14})$$

$$\Gamma_{121} = \Gamma_{211} = \frac{N_t k_B T_0}{2} \left[\frac{\epsilon_\beta \tau_\beta}{(1 - x^1)^2} + \frac{2 \epsilon_\alpha \tau_\alpha x^1}{(1 - x^2)^3} \right], \quad (\text{S15})$$

$$\Gamma_{122} = \Gamma_{212} = \frac{N_t k_B T_0}{2} \left[\frac{\epsilon_\alpha \tau_\alpha}{(1 - x^2)^2} + \frac{2 \epsilon_\beta \tau_\beta x^2}{(1 - x^1)^3} \right], \quad (\text{S16})$$

$$\Gamma_{221} = \frac{N_t k_B T_0}{2} \left[\frac{\epsilon_\beta \tau_\beta}{(1 - x^1)^2} + \frac{2 \epsilon_\alpha \tau_\alpha x^1}{(1 - x^2)^3} + \frac{4}{3} \cdot \frac{\epsilon_\alpha \epsilon_\beta \tau_h}{(1 - x^1)(1 - x^2)^2} \right], \quad (\text{S17})$$

$$\Gamma_{112} = \frac{N_t k_B T_0}{2} \left[\frac{\epsilon_\alpha \tau_\alpha}{(1 - x^2)^2} + \frac{2 \epsilon_\beta \tau_\beta x^2}{(1 - x^1)^3} + \frac{4}{3} \cdot \frac{\epsilon_\alpha \epsilon_\beta \tau_h}{(1 - x^2)(1 - x^1)^2} \right]. \quad (\text{S18})$$

In Eq. (S11), we have $\Gamma_{jk}^i \equiv g^{li} \Gamma_{jkl}$ with the inverse metric g^{ij} . We apply the shooting method [1] in searching of the geodesic path with a target point $(\epsilon_\alpha, \epsilon_\beta)$. The boundary value problem of the ordinary differential equation is converted into an initial value problem by adding the initial derivative $x^{i'}(0)$ into the initial condition. A proper value of $x^{i'}(0)$ is searched to allow the end of solved geodesics path match the target point $(\epsilon_\alpha, \epsilon_\beta)$. We represent the solved geodesics path as a function of the arc length r , i.e., $x^i = x^i(r)$, $0 < r < \mathcal{L}$, and \mathcal{L} is the thermodynamics length of the path. To represent the protocol $\tilde{x}_{L,R}(s)$, we can re-parameterize $x^i(r)$ by $s \equiv r/\mathcal{L}$, and the protocol is explicitly $\tilde{x}_L(s) = x^1(s\mathcal{L})$, $\tilde{x}_R(s) = x^2(s\mathcal{L})$.

It is worth noting that the metric at $(\epsilon_\alpha, \epsilon_\beta)$ is degenerate

$$G = N_t k_B T_0 \left(\tau_\alpha + \tau_\beta + \frac{2}{3} \cdot \tau_h \right) \begin{pmatrix} 1 & 1 \\ 1 & 1 \end{pmatrix},$$

inducing the divergence of G^{-1} . And the Christoffel symbols Γ_{ij}^k are also divergent at the target point $(\epsilon_\alpha, \epsilon_\beta)$. When numerically solving the geodesic equations, we set the target point $(\epsilon_\alpha, \epsilon_\beta) = (0.5, 0.5)$. Due to the divergence of $\Gamma_{\mu\nu}^\rho$,

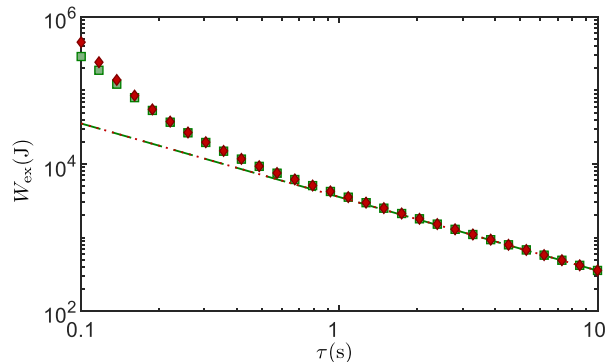


Figure S1. Excess work W_{ex} versus operation time τ in the short time region. The red diamonds (green squares) represent the irreversible work obtained by solving the evolution equation of the system along the symmetric (symmetry-breaking) path. The red dashed line (green solid line) represents the excess work predicted by the thermodynamic length $W_{\text{ex}} = \mathcal{L}^2/\tau$.

the integral step length δr is supposed to decrease to meet the accuracy requirement. The solving procedure stops once the required step length is smaller than a minimum one, set by our algorithm. There is a small distance between the stop point and the target point. In the numerical calculation of the geodesic equation, we set the minimum step length to be $\delta r_{\text{min}} = 10^{-13}(\text{J} \cdot \text{s})^{1/2}$, and obtain a stop point with a Euclidean distance 9.7×10^{-8} away from $(0.5, 0.5)$, or a geometric distance $\Delta \mathcal{L} \approx 4.9 \times 10^{-6}(\text{J} \cdot \text{s})^{1/2}$ (the relative error of the thermodynamic length of the whole path is $\Delta \mathcal{L}/\mathcal{L}_{\text{geo}} \approx 8.2 \times 10^{-8}$). This distance is small enough to be ignored.

VI. SINGULARITIES OF THE EVOLUTION EQUATIONS

With the protocol $\tilde{x}_{L,R}(s)$ obtained from the geodesic path, we can numerically simulate the evolution of the ideal gas by the evolution Eqs. (15)-(17) of the main text. With a certain operation time τ , the volumes are expressed explicitly $V_k(t) = V_t \tilde{x}_k(t/\tau)$ as functions of time. The evolution equations have two removable singularities at the beginning $t = 0$ and the end $t = \tau$ of the separation process, since the particle densities $N_{\sigma k}/V_k$ become in the form $0/0$. The singularities will bring computational difficulty for the numerical simulation. Here we illustrate how to avoid the singularities in the numerical simulation without affecting the final result.

At the beginning $t = 0$ of the separation process, the particle densities $N_{\alpha L}/V_L$ and $N_{\beta R}/V_R$ of the left and the right compartments lead to a removable singularity of the evolution equations since both the numerators and denominators approach 0. We consider an initial equilibrium state of the gas, and thus the initial values of the molecular numbers are given by Eqs. (S7) and (S8). In the numerical simulation, this singularity can be avoided by choosing an initial time slightly larger than zero, such as $\delta t_i = \tau \times 10^{-8}$. The initial V_k is slightly larger than zero by $V_k(\delta t_i)$, and the initial $N_{\sigma k}$ is set according to Eqs. (S7) and (S8). We also remark that in real situation the volumes cannot be perfectly zero.

At the end $t = \tau$ of the separation process, the particle densities $(N_{\alpha} - N_{\alpha L})/(V_t - V_L - V_R)$ and $(N_{\beta} - N_{\beta R})/(V_t - V_L - V_R)$ of the middle compartment lead to a removable singularity of the evolution equations. The final point obtained by the shooting method is not exactly $(0.5, 0.5)$. And the volume of the middle compartment has a small positive value at the end of the separation process. Thus, the differential equations can be solved numerically with the protocol obtained from the shooting method.

VII. EXCESS WORK FOR SHORT OPERATION TIME

The above discussion on the excess work is for the long time region where the operation time τ is much larger than the time scale of relaxation. In the short-time region, we show the excess work in Fig. S1 with numerical simulation. The red diamonds (green squares) represent the irreversible work obtained by solving the evolution equation of the system for the symmetric (symmetry-breaking) protocol. The red dashed line (green solid line) represents the excess work predicted by the thermodynamic length $W_{\text{ex}} = \mathcal{L}^2/\tau$. The excess work is far larger than the reversible work $W^{(0)}$ in Sec. II.

* hdong@gscaep.ac.cn

[1] M. Berger, *A Panoramic View of Riemannian Geometry* (Springer Berlin Heidelberg, 2007).